


Article

Numerical Investigation of Thermo-Flow Characteristics of Tubes with Transverse Micro-Fins

Piotr Bogusław Jasiński 

Institute of Turbomachinery, Lodz University of Technology, Wólczajska Str. 217/221, 93-005 Łódź, Poland; piotr.jasinski@p.lodz.pl; Tel.: +48-42-631-23-49

Abstract: The article presents the results of numerical studies of heat transfer and pressure drops in a channel with transverse micro-fins. The main aim of the study was to prepare the thermal and flow characteristics of such a channel for a variable longitudinal spacing of micro-fins. For the tested pipe with an internal diameter of $D = 12$ mm, the absolute height of the micro-fins was $e = 0.243$ mm, which is 2% of its diameter. The tests were carried out for turbulent flow in the range of Reynolds numbers of 5000–250,000 with the variable spacing of micro-ribs in the range of $L = 0.28$ –13.52 mm, which corresponds to their dimensionless longitudinal distance, $L/D = 0.023$ –1.126. For the studied geometries, the characteristics of the friction factor, $f_t(Re)$, and the Nusselt number, $Nu(Re)$, are shown in the graphs. The highest values of Nu were observed for a spacing of $L/D = 0.092$ in the range of $Re = 5000$ –60,000, while the lowest were observed for a geometry of $L/D = 0.035$ for $Re = 60,000$ –250,000. The friction factors, however, were the highest for the two geometries $L/D = 0.161$ and $L/D = 0.229$ over the entire range of the tested Re numbers. A large discrepancy was observed between the friction factors calculated from the Colebrook–White equation (for irregular relative roughness depicted in the Moody diagram) and those obtained from simulations (for pipes with the same roughness height but regular geometry created by micro-fins). An analysis of the heat transfer efficiency of the tested geometries was also presented, taking into account the criterion of equal pumping power, i.e., the PEC (performance evaluation criteria) coefficient. The highest values of the PEC coefficient, up to 1.25–1.28, were obtained for micro-fin spacings of $L/D = 0.069$ and $L/D = 0.092$ in the Re number range of 20,000–30,000.



Citation: Jasiński, P.B. Numerical Investigation of Thermo-Flow Characteristics of Tubes with Transverse Micro-Fins. *Energies* **2024**, *17*, 714. <https://doi.org/10.3390/en17030714>

Academic Editors: Hongbing Ding, Yasser Mahmoudi Larimi, Mohammad Jadidi and Mohammadhadi Hajilou

Received: 14 November 2023
Revised: 28 January 2024
Accepted: 30 January 2024
Published: 2 February 2024



Copyright: © 2024 by the author. Licensee MDPI, Basel, Switzerland. This article is an open access article distributed under the terms and conditions of the Creative Commons Attribution (CC BY) license (<https://creativecommons.org/licenses/by/4.0/>).

Keywords: heat transfer coefficient; transverse micro-fins; pipe; friction factor; numerical methods; PEC ; CFD

1. Introduction

A pipe, as a flow channel, is one of the simplest and most frequently used solutions in the energy industry and thermal devices. It has many applications, from heat exchangers to transporting media in installations. The phenomena occurring there concern both fluid mechanics and thermal processes; therefore, the key aim is to design its geometry in such a way as to maximize heat transfer while limiting the negative phenomenon of flow resistance.

There are many flow channel geometries and methods for intensifying heat transfer as fluid flows through these channels. Among other things, intensifying inserts of various shapes and other flow turbulizing devices are widely used [1–5]. Yet another way is to modify the physical properties of the working fluid by adding nanoparticles [6–9], and yet another way is to fin the internal surface of the channels in various ways, including the way that is presented in this article.

In the available literature, you can find many research papers on similar geometry. Most of them are experimental, but there are more and more publications based on numerical research or combining these two forms of research. For example, Virgilio et al. [10] investigated the use of 2D and 3D helical inserts to observe the turbulence induced by

these inserts and the associated flow resistance. They found that the friction coefficients of the tested continuous and discontinuous turbulators are seven and four times higher, respectively, than those of a smooth pipe for the same Re number. Ji et al. [11] conducted an experiment for developed turbulent flow in the range of $Re = 10,000$ – $100,000$ for 16 different pipes with internal grooves. They compared the experimental results with an analytical method using the Gnieliński equation, which was then extended by the Nusselt number. The proposed extended equation gave good agreement with the results, where the deviation for 93% of the data was within $\pm 20\%$. Córcoles et al. [12] performed numerical simulations to analyze the influence of geometric parameters on eight spiral internal corrugated tubes in a double-pipe heat exchanger with a turbulent flow of up to $Re = 50,000$. Various combinations of pitch and corrugated heights were tested in a three-dimensional numerical model of the pipe and also verified using an experimental system. The highest PEC value of 1.12 was observed for grooves with a height-to-diameter ratio of $H/D = 0.032$. Al-Obaidi et al. [13,14] studied the thermal flow characteristics of various geometries of 3D corrugated pipes with H/D corrugation heights of up to 10%. The results show that the corrugated surface improves the flow disturbance in the wall region, which leads to an increase in induced vortices, increasing convective heat transfer and improving the overall pipe performance. For the studied geometries, the highest PEC s were obtained for small Re numbers, approximately 4000. Dastmalchi et al. [15] optimized the geometry of micro-finned tubes using numerical methods to increase heat transfer and minimize flow resistance. They studied pipe-in-pipe heat exchangers during turbulent flow, changing the geometric parameters of the tube, i.e., the internal diameter, the number of fins, and their height, for values of Re from 3000 to 100,000. They noticed, among other things, that the optimal micro-fin height increases with increasing Re for all the considered pipe internal diameters. Also, Dastmalchi et al. [16] performed oil flow tests at low values of Re , from 100 to 1000, in a pipe with internal micro-fins. As before, they examined the influence of pipe geometry on heat transfer efficiency and flow resistance. The example results for $Re = 1000$ show a maximum increase in heat transfer of 44% but also an increase in the friction factor of 69% for flow through pipes with micro-fins compared to flow through a smooth pipe. Jasiński [17] used a numerical simulation to model the flow in an internally finned pipe for various micro-fin helical angles in the range of $0 \div 90^\circ$. Using the EGM (Entropy Generation Minimization) method to evaluate the flow, he showed that for each geometry, the minimum entropy is generated for the range $Re = 60,000 \div 90,000$. Li et al. [18] investigated the mechanism of heat transfer enhancement by turbulence in transverse corrugated pipes with different corrugation heights. They found that the heat transfer characteristics were related to the relative magnitudes of the corrugation height and the viscous sublayer thickness, and they obtained the best heat transfer enhancement at a roughness height approximately three times greater than the viscous sublayer thickness. Brognaux et al. [19] developed the characteristics of a single-phase flow through a pipe with two types of internal fins. They analyzed the influence of geometry on the Prandtl number and determined the dependence of the friction factor on the Reynolds number. From the experimental results, they observed that the Prandtl exponent agrees well with other correlations for geometries with two-dimensional roughness.

The presented paper attempts to investigate the problem of the thermal efficiency of several geometries of pipes with transverse micro-fins. By changing the distances between them, the highest PEC values were sought while maintaining the same pumping power.

2. Materials and Methods

2.1. Experimental Validation of the CFD Code

Before performing numerical simulations, tests were performed on an experimental stand for one of the pipe geometries, and the results obtained from the experiment were used to validate the numerical model. The object of the research was an internal finned pipe, industrially produced by KME Germany AG & Co. KG with the working name "TECTUBE fin 12736CV50/65D" and dimensions given in Figure 1. It is used, among

others, to produce heat exchangers, both in single-phase and two-phase flow. The exact procedures and descriptions of the experimental tests are presented in [20]. The tested pipe had a different arrangement of micro-fins (longitudinal helical) but the same micro-fin geometry (i.e., angle α , diameter, height, and width of the base) as the object studied numerically in this article.

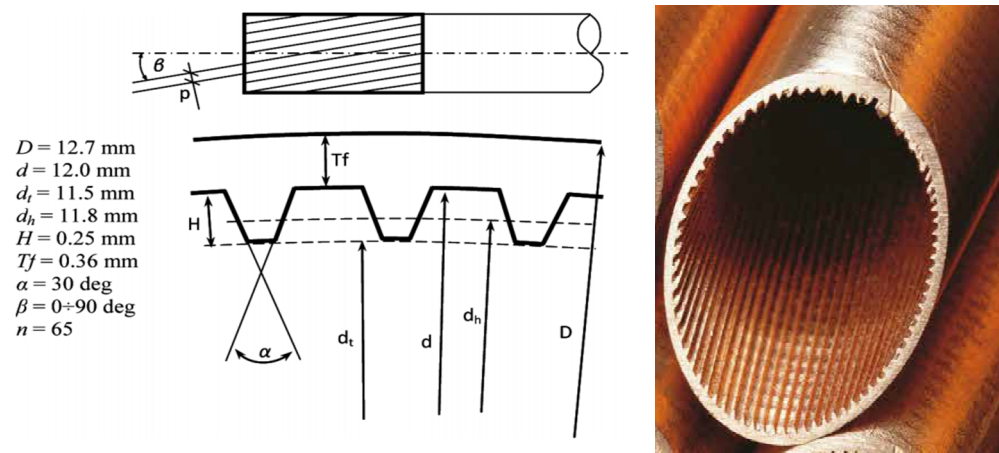


Figure 1. Schematic diagram and dimensions of the micro-finned pipe “TECTUBE fin 12736CV50/65D” from KME Germany AG & Co. KG.

Figure 2 compares the results of the experiment and the numerical tests for a micro-finned pipe. In this procedure, the two most popular turbulence models were also validated: the classical $k-\epsilon$ and SST $k-\omega$ methods. The graphs clearly show that the best agreement with experimental values, both for pressure drop and heat transfer, was obtained using the SST $k-\omega$ turbulence model. Therefore, this model was used for further numerical calculations.

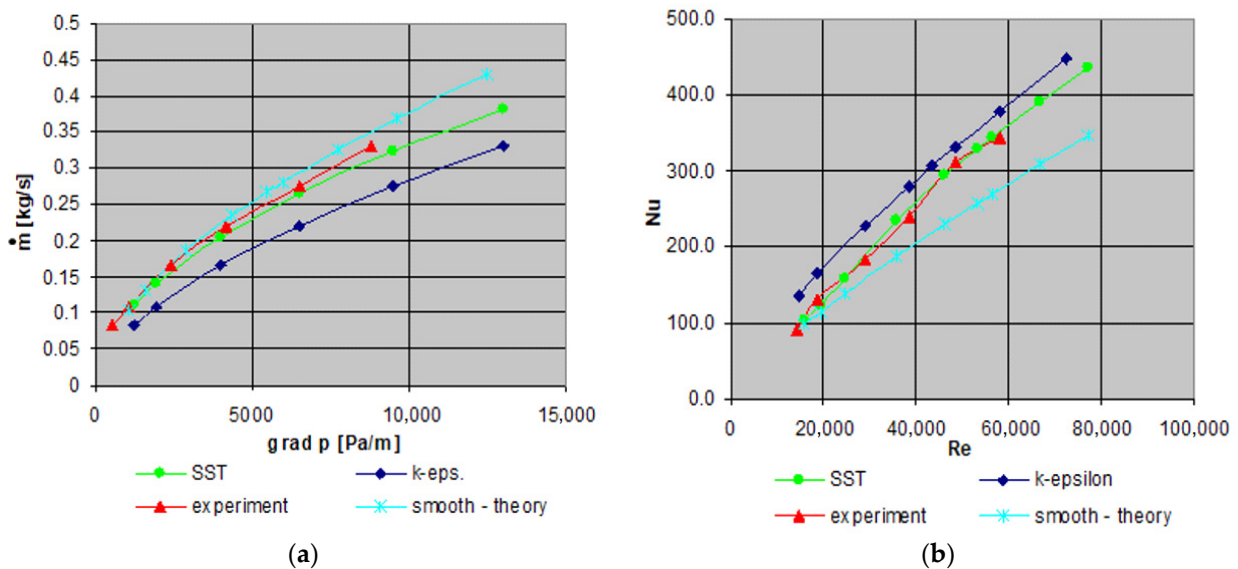


Figure 2. Comparison of the results of numerical simulation and experiment for the micro-fin tube and for the SST $k-\omega$ and $k-\epsilon$ turbulence models used: (a) mass flow vs. $\text{Grad}p$ and (b) Nu vs. Re [11,12].

2.2. Geometrical Model

The purpose of the numerical calculations was to study the thermal and flow characteristics of pipes with internal micro-fins perpendicular to the direction of fluid flow. As mentioned earlier, compared to the experimentally tested industrial pipe “TECTUBE fin

12736CV50/65D” shown in Figure 1, in the numerically analyzed pipe, the direction of the micro-fin arrangement was different, but their dimensions were the same. Consequently, the relative roughness of the pipe, which is defined as the ratio of the roughness height to its diameter, $\epsilon = e/D$, was also the same. In the tested pipes, the only variable geometric parameter was the longitudinal distance between the micro-fins, L , which was varied in the range of 0.28–13.52 mm, as shown in Figure 3. Table 1 shows all the geometric parameters of the tested pipes, including the dimensionless distances between micro-fins, defined as the ratio L/D , and their corresponding geometry designations. Figure 4 shows example geometries of the analyzed pipes, maintaining their scale in relation to their diameter and micro-fin height.

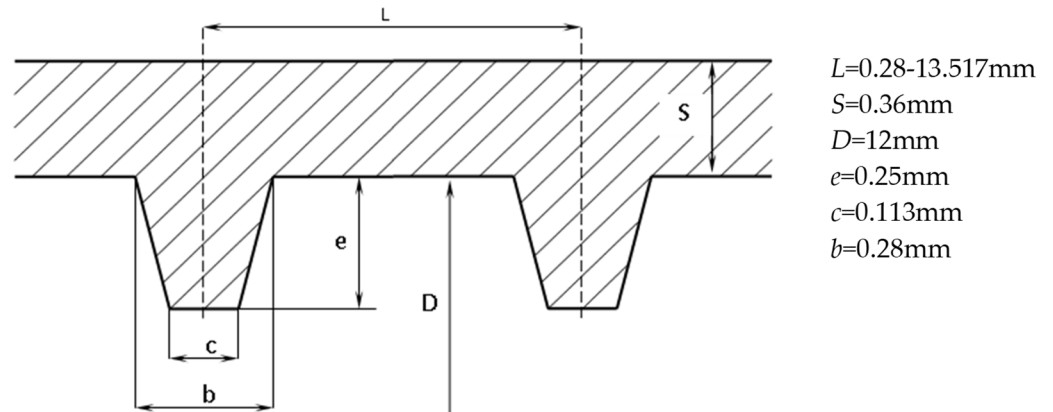


Figure 3. Geometrical dimensions of tested micro-fin tube.

Table 1. Longitudinal spacing of micro-fins and markings of the tested geometries.

L [mm]	0.28	0.418	0.555	0.831	1.107	1.934	3.598	6.898	13.517
L/D [-]	0.023	0.035	0.046	0.069	0.092	0.161	0.299	0.575	1.126
name of geometry	X1	X2	X3	X4	X5	X6	X7	X8	X9

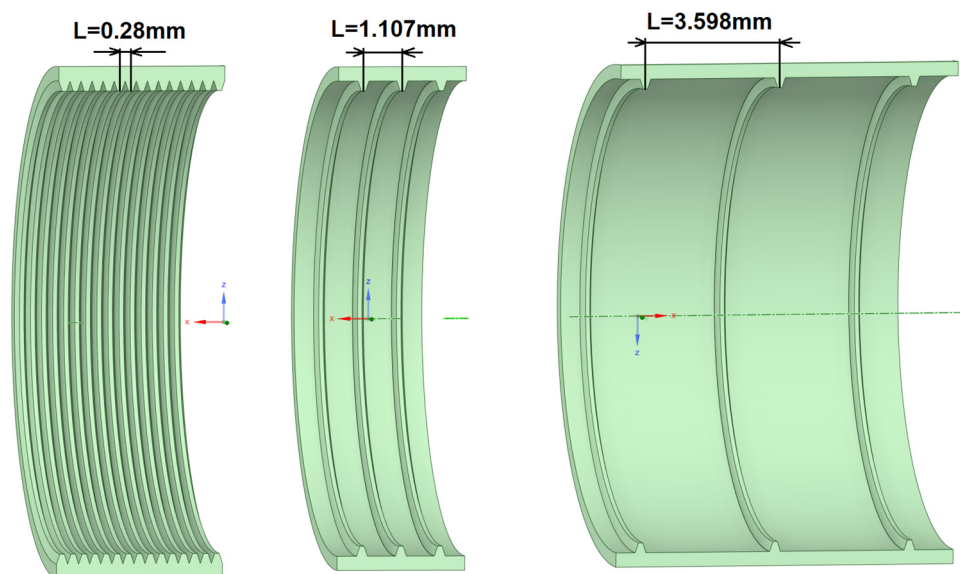


Figure 4. Example of pipe geometries with different longitudinal spacings of micro-fins. From the left: X1, X5, and X7, respectively.

2.3. Numerical Model and Boundary Conditions

A repeating fragment of pipe geometry with an opening angle of 30° and a length corresponding to the longitudinal spacing L was used as the computational domain, as shown in Figure 5. Instead of the whole long pipe, its repeatable, periodic, and axially symmetrical fragment was used for the calculations, representative of the entire channel and reflecting the same flow and thermal phenomena. This approach to the problem is correct if the flow obtained is fully developed, both hydraulically and thermally. As we know, under normal conditions, a fully developed flow can only be achieved over a pipe length of approximately 40–50 diameters from its inlet. If a short, repeating section of the domain is used, appropriate boundary conditions must be applied in the CFD calculation code to obtain such a flow structure. For this purpose, translational periodicity was used at the inlet and outlet of the domain, and the fluid flow was forced by a pressure gradient corresponding to an Re number range of $5000 \div 250,000$. Axial symmetry was used on the side surfaces of the domain. The concept of reducing the domain size, and thus also the number of nodes in the computational mesh, allows for a significant reduction in computation time while maintaining the high quality of the mesh and the results' accuracy. This research method has also been presented in many works, including [1–3,21].

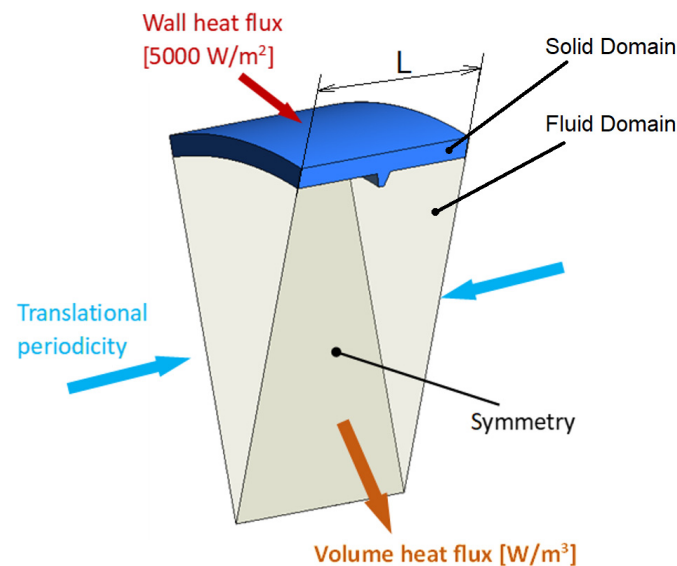


Figure 5. Boundary conditions in the numerical model.

Table 2 shows a detailed summary of the boundary conditions for the numerical model. The numerical model consisted of two computational domains. In the flow domain, water was defined as the working fluid, with an average temperature of 298 K, while the solid domain was copper. Additionally, to obtain a fully thermally developed flow and calculate the correct temperature field, a negative volumetric heat source was set in the fluid domain (1), which allowed us to balance the thermal energy supplied to the domain wall by a surface heat flux of $q = 5000 \text{ W/m}^2$.

$$-\dot{Q}_{\text{vol}} = \frac{q \cdot A_{\text{wall}}}{V_{FD}} \left[\frac{\text{W}}{\text{m}^3} \right] \quad (1)$$

All numerical simulations were performed using the commercial software ANSYS-CFX v.18.1 [22].

Table 2. Parameters of boundary conditions.

Boundary Condition	Description	Parameter	Value
Fluid domain	Water	Average temperature	298 K
		Reference pressure	1 atm
		Turbulence model	SST k- ω
		Volume heat flux	$-\dot{Q}_{vol} \frac{W}{m^3}$
Solid domain	Copper.	Average temperature	298 K
Wall	Top surface of solid domain	Wall heat flux	5000 $\frac{W}{m^2}$
Translational periodicity	Inlet and outlet of fluid domain.	Pressure gradient	76–57,900 Pa/m

2.4. Turbulence Model

The SST k- ω (Shear Stress Transport) turbulence model is one of the most popular models used in many CFD applications. Its main attribute is its ability to solve the viscous sublayer by applying the k- ω model in the boundary sublayer and the standard k- ϵ model in the turbulent core region. “Switching” between the two models is controlled by a built-in special blending function [22–24]. The correct use of the SST model requires several grid points within this sublayer to maintain the dimensionless distance condition $y^+ < 2$ throughout the computational domain [22]. This value was not exceeded in any of the geometries tested.

One of the criteria for the uniqueness of the numerical solution was to achieve appropriate convergence for the residuals: momentum, energy, and turbulence. In all the simulations, a convergence of approximately 10×10^{-4} was achieved for the maximum residuals and an order of magnitude lower (10×10^{-5}) for the average residuals (RMS). The second criterion for the unambiguity of the solution was the stabilization of the flow and thermal parameters, such as speed, pressure, and temperature, which were monitored both as average values and at several selected points in the computational domain. The calculation process was stopped if the above parameters did not change for several subsequent iterations.

2.5. Mesh Independence Study

Before the actual simulations, checking calculations were performed for several geometries with different mesh densities. For further calculations, a structural and hexagonal mesh of such a density at which a higher density gives results that differ by less than 1% was selected.

Figure 6 shows an example of checking the independence of the mesh for two tested parameters related to heat transfer and flow resistance. Meshes with numbers of nodes of 1.16×10^5 , 8.1×10^5 , 1.23×10^6 , 1.653×10^6 , and 2.12×10^6 were tested. As can be seen, as the mesh density increases, Nu decreases, and the friction factor increases. In this case, a mesh with 1.653×10^6 nodes was selected because the next mesh with 2.12×10^6 nodes gave results that differed from the previous one by the above criterion. Since each tested geometry has a different size, the same procedure was performed for all the geometries used to test the independence of the grid, successfully achieving the established independence criteria.

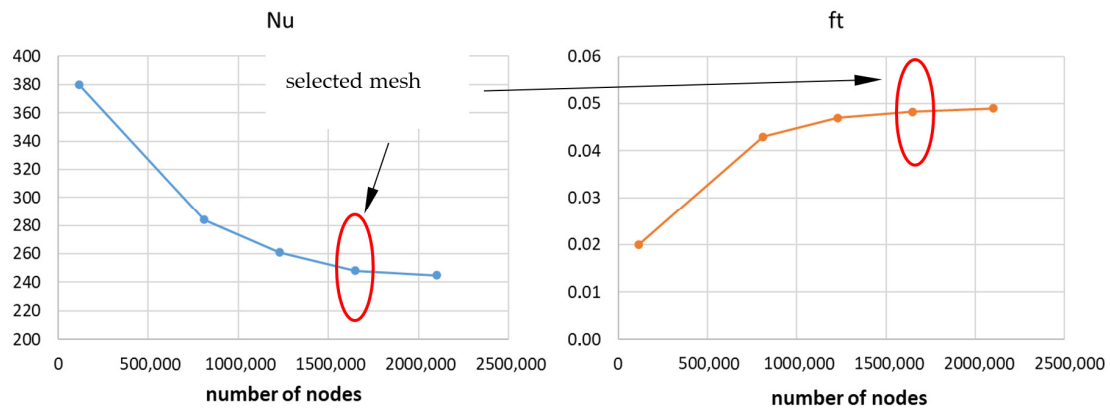


Figure 6. Mesh independence test for X5 sample geometry.

For all the geometries, attempts were made to maintain a computational mesh with approximately the same average cell volume. In the area of the hydraulic boundary layer, the mesh was additionally densified to obtain the appropriate value of the y^+ coefficient. After testing, it could be concluded that the mesh used and the test results are independent of its density, consistent with the recommendations in [25].

Figure 7a shows an example of a low-quality (coarse) computational mesh, and Figure 8a shows a densified, medium-quality mesh. In the low-quality mesh, the total number of nodes in the fluid domain was 1.16×10^5 , while in the compacted mesh, it was about 8.12×10^5 . In addition, the average dimensions of the mesh cells in the near-wall layer were about 0.065×0.032 mm and 0.018×0.018 mm for the coarse and medium mesh, respectively. The density of the mesh in the near-wall layer is important for the y^+ value obtained, as can be seen in Figures 7b and 8b, where its distribution on the domain wall is shown. Under the same flow conditions, the highest y^+ values occur at the top of the micro-fin, i.e., at the location of the highest fluid velocity. As can be seen, the maximum value is $y^+ = 4.9$ for the coarse mesh and $y^+ = 1.68$ for the medium mesh. As mentioned earlier, using the SST $k-\omega$ turbulence model, $y^+ < 2$ should be maintained, which, in this case, is met by the medium mesh.

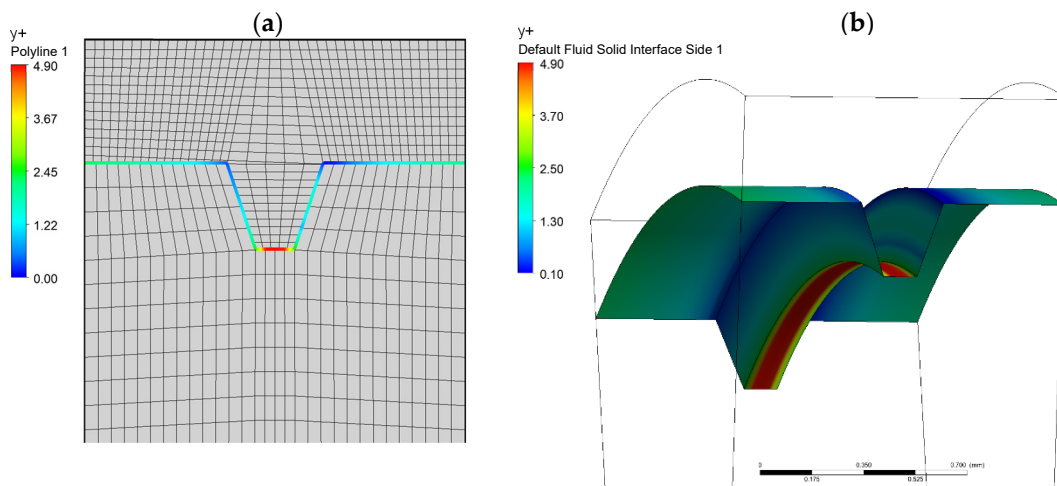


Figure 7. View of the near-wall area in the computational domain—coarse mesh (a), y^+ distribution on the domain wall (b). Flow conditions for $Re = 80,000$.

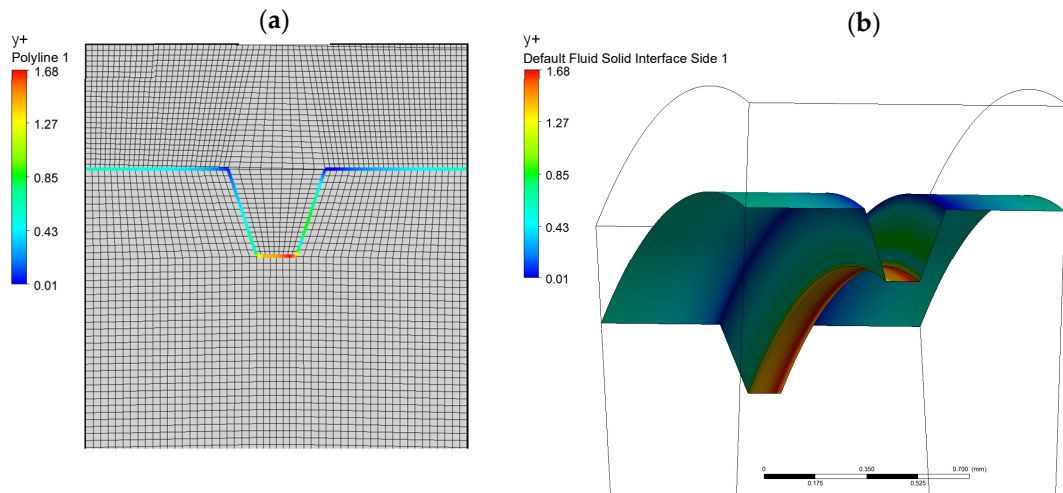


Figure 8. View of the near-wall area in the computational domain—medium mesh (a), y^+ distribution on the domain wall (b). Flow conditions for $Re = 80,000$.

3. Results

3.1. Data Processing

The use of any micro-fins in a flow channel always increases the flow resistance compared to the flow in a smooth pipe. For a given pipe diameter, these resistances depend mainly on the geometry of the micro-fins, their arrangement, and the average fluid flow velocity.

In the numerical calculations, the pressure gradient described by Equation (2) was used to force the flow:

$$\text{grad}p = \frac{\Delta p}{L} = ft \cdot \frac{\rho \cdot u_{av}^2}{2 \cdot D} \quad (2)$$

For each tested geometry, the friction factor was calculated using the Darcy–Weisbach equation in Equation (3), which is a modification of Equation (2):

$$ft = \frac{2 \cdot D}{\rho \cdot u_{av}^2} \cdot \frac{\Delta p}{L} \quad (3)$$

Re is defined as a function of the average velocity, u_{av} , in the pipe cross-section and its diameter, D :

$$Re = \frac{u_{av} \cdot D}{\nu} \quad (4)$$

The theoretical value of the friction factor for a smooth pipe, as a reference level for the numerical results, was calculated from the Blasius correlation (5):

$$ft_s = 0.3164 \cdot Re^{-0.25} \quad (5)$$

To calculate Nu from the numerical simulations, the relationship (6) was used:

$$Nu = \frac{h \cdot D}{k} \quad (6)$$

where the heat transfer coefficient, h , was determined from the obtained numerical results and substituted into Equation (7):

$$h = \frac{q}{T_w - T_b} \quad (7)$$

Similarly, the Nusselt number was calculated for a smooth pipe based on the well-known Dittus–Boelter Equation (8):

$$Nu_s = 0.023 \cdot Re^{0.8} \cdot Pr^{0.4} \quad (8)$$

The *PEC* coefficient, on the other hand, according to the criterion of a constant pumping power, was calculated from the relationship:

$$PEC = \frac{Nu/Nu_s}{(ft/ft_s)^{\frac{1}{3}}} \tag{9}$$

3.2. Friction Factor

For each pipe geometry, 16 numerical simulations were performed for different Reynolds numbers. The set value forcing the flow was the pressure gradient, $gradp$, and the average velocity in the pipe, u_{av} , was the result of numerical calculations and depended on the flow resistance. The results of the numerical simulations, in the form of characteristics of the friction factor, $ft(Re)$, are shown in Figure 9. The curve for a smooth pipe, calculated from the Blasius correlation (5), is also plotted on this graph to show the reference level.

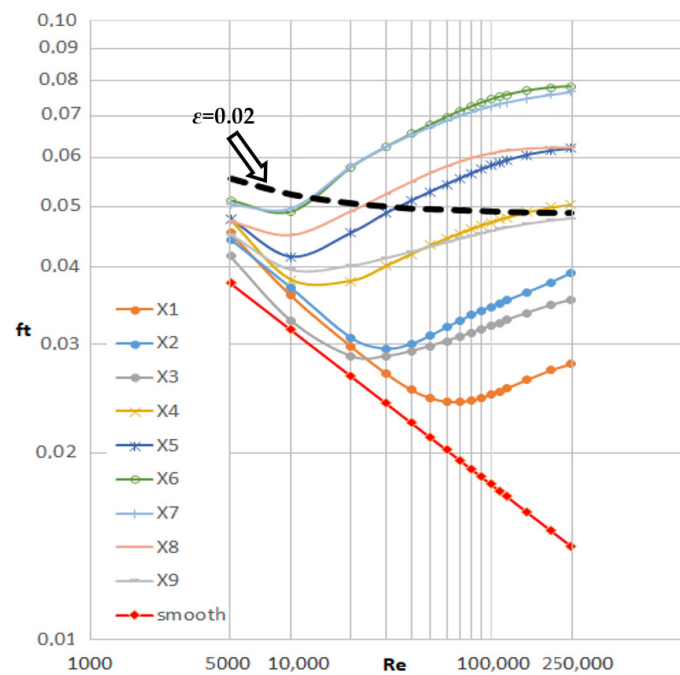


Figure 9. Friction factor, $ft(Re)$, for the tested geometries as a function of Re .

Observing the ft characteristics in Figure 9, one notices their different positions in relation to a smooth pipe and even to a pipe with irregular roughness but the same relative roughness ($\epsilon = e/D = 0.02$) as the tested micro-fin geometries. The characteristics in the graph show that as the Re increases, the friction factors initially decrease and then increase. These curves create a minimum for the Re number range, which is different for each geometry. The mathematical analysis showed that the only formula that gives the best correlation with the numerical results is a third-order exponential decay function (10). The calculated correlation coefficients of this function for each geometry are given in Table 3.

$$ft = y_0 + A_1 \cdot \exp\left(\frac{-(Re - x_0)}{t_1}\right) + A_2 \cdot \exp\left(\frac{-(Re - x_0)}{t_2}\right) + A_3 \cdot \exp\left(\frac{-(Re - x_0)}{t_3}\right) \tag{10}$$

Table 3. Fitting parameters for Equation (10).

	X1	X2	X3	X4	X5	X6	X7	X8	X9
y_0	0.02885	0.049	0.03662	0.03662	0.06238	0.07841	0.15778	0.06223	0.04878
x_0	−688.1	6974.9	1806.7	1806.7	3924.9	11,555.1	8866.9	7953.6	13,540.9
A_1	0.02543	0.03526	0.03176	0.03176	−0.03265	−0.01287	−0.08415	−0.0369	−0.00266
t_1	22,095.0	12,504.6	5123.8	5123.8	5937.5	50,738.5	6,715,600	35,397.1	221,583.0
A_2	0.0465	−0.02554	−0.00401	−0.00401	−0.02041	−0.00965	−0.00845	0.01572	−0.00349
t_2	3075.3	20,253.3	5123.9	5123.9	60,471.8	50,714.8	7969.5	35,397.1	53,562.3
A_3	−0.01114	−0.01788	−0.01024	−0.01024	0.04278	−0.0052	−0.01772	0.00274	−0.00338
t_3	105,718.5	421,954.3	121,313.7	121,313.7	3961.4	6729.3	43,461.64	35,397.2	53,565.9

The analysis of the obtained results allowed us to observe a large deviation from the characteristics of rough pipes presented in Moody’s chart [26]. As mentioned earlier, the relative roughness is defined as the ratio of the height of the roughness to the diameter of the pipe (11), which is constant for the tested geometries and amounts to 0.02.

$$\varepsilon = \frac{e}{D} \quad (11)$$

The friction factor for surfaces with irregular roughness was calculated using the empirical Formula (12) [27] and is shown in a graph against the tested pipes; see Figure 9.

$$ft = \frac{0.25}{\left(\log\left(\frac{e}{3.7 \cdot D} + \frac{5.74}{Re^{0.9}}\right)\right)^2} \quad (12)$$

Despite the fact that the analyzed pipes meet the conditions of a relative roughness of 0.02, it is not possible to calculate their friction factor from Equation (12). Figure 9 shows the total divergence of the curves obtained from the numerical simulations compared to those calculated theoretically. Therefore, one of the main conclusions resulting from the conducted research is the fact that for regular shapes of micro-fins, the decisive influence on the friction factor comes from their geometry and arrangement, not only their height. The same fact was noticed in research by Wang et al. [28].

Figure 10 shows the dependence of the friction factor on the micro-fin spacing for several selected values of Re . As can be seen, the highest values of ft for all Re values can be observed for a spacing of about $L/D = 0.16$ – 0.29 , which corresponds to the geometry of the tubes labeled X6 and X7. It can therefore be concluded that these micro-fin spacings give the highest flow resistance. However, the smallest ft values occur for the smallest L/D spacing, i.e., for geometries X1 to X4.

3.3. Heat Transfer

Figure 11 shows the thermal characteristics for all the tested pipe geometries in the form of the $Nu(Re)$ function, as well as one characteristic for a smooth pipe calculated from (8) as a reference level. For the presented thermal characteristics, a power approximation function (13) was fitted, where, similarly to (8), Nu is a function of Re and Pr . Due to the significant deviation of the correlation from the measurement data for large values of Re , Formula (13) gives a good function fit only for $Re < 100,000$. Table 4 gives the correlation coefficients A and B of the power function for each geometry.

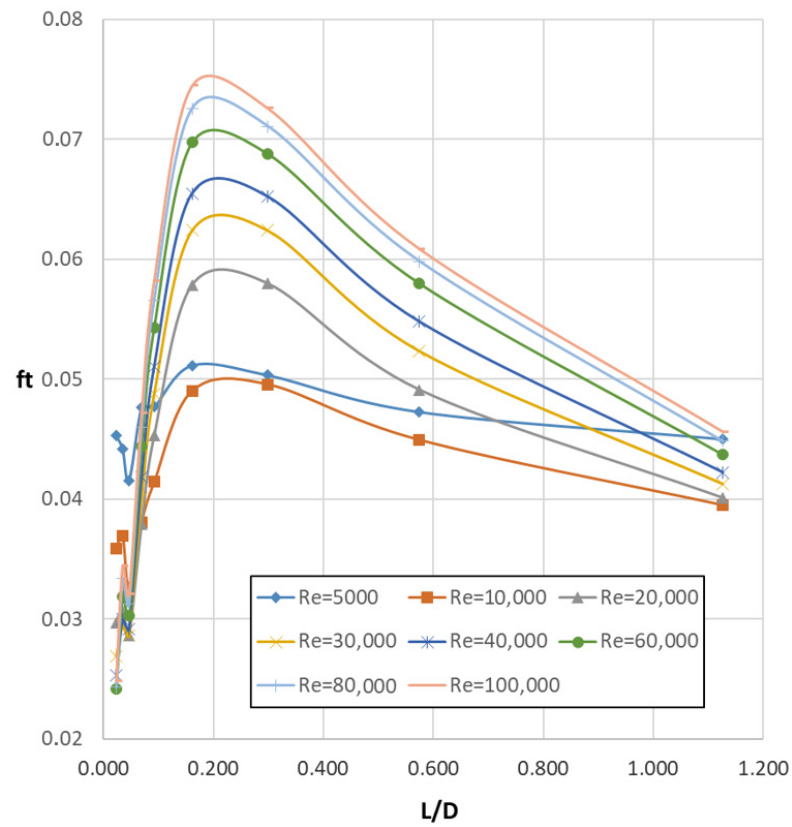


Figure 10. Friction factor, f_t , of the tested geometries as a function of L/D spacing.

$$Nu = A \cdot Re^B \cdot Pr^{0.4} \tag{13}$$

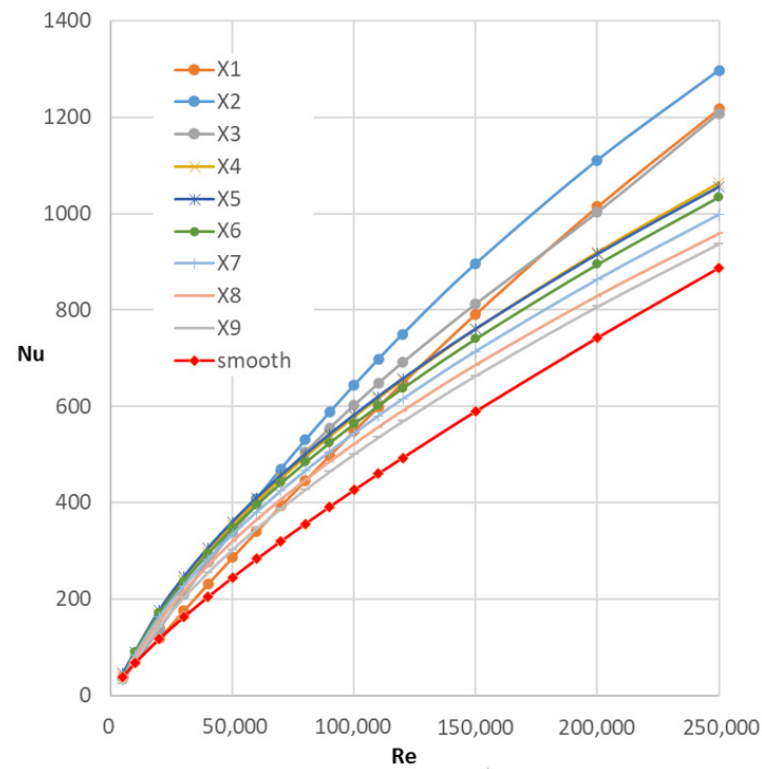


Figure 11. Nusselt number as a function of the Reynolds number, $Nu(Re)$, of the studied geometries.

Table 4. Fitting parameters for Equation (12).

	X1	X2	X3	X4	X5	X6	X7	X8	X9
A	0.01	0.0065	0.0072	0.0138	0.0206	0.0137	0.0093	0.0061	0.0055
B	0.892	0.948	0.935	0.878	0.843	0.877	0.908	0.944	0.948

Figure 11 shows the thermal characteristics of the studied geometries. As can be seen, in the range of Re from about 70,000 to 250,000, the highest Nu values are reported for geometry X2. In the range of smaller Re values $< 70,000$, the largest values of Nu were obtained for the X5 geometry.

3.4. PEC (Performance Evaluation Criteria)

In a pipe with internal micro-fins, the key thermal flow phenomena take place in the boundary layer, which can be visually defined as the space between the micro-fins and the pipe wall and above the tops of the micro-fins. Both the flow resistance and the heat transfer process on the wall are strictly dependent on the pipe geometry, i.e., the longitudinal spacing of the micro-fins. Figure 12 shows the temperature fields in the axial section of the pipe for three sample geometries: X2, X5 and X7. Figure 13 shows the corresponding velocity fields.

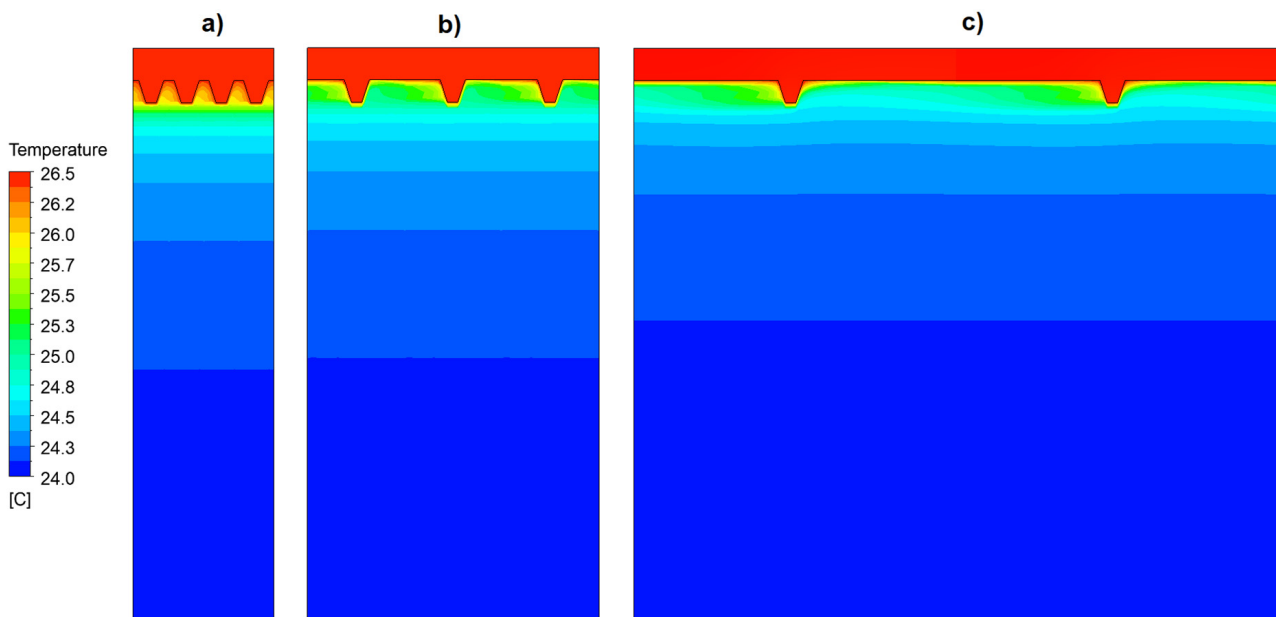


Figure 12. Temperature field for selected geometries at the same pressure gradient of 1000 [Pa/m]: (a) X2, (b) X5, and (c) X7.

Figure 14 shows an example of the distribution of turbulence intensity (Turbulence Kinetic Energy, TKE) in the flow through the selected geometries. In the analyzed cases, the highest values of this parameter are located in the region a little away from the top of the micro-fin. The TKE decreases gradually in the direction of the wall as well as in the direction of the pipe axis as the vortices disappear. Among the selected geometries, the highest values are recorded for X5 (max. $1.4 \times 10^{-2} \text{ m}^2/\text{s}^2$), while it can be seen that for X7, the area of the max. turbulence shifts and partially disappears in the area between the micro-fins.

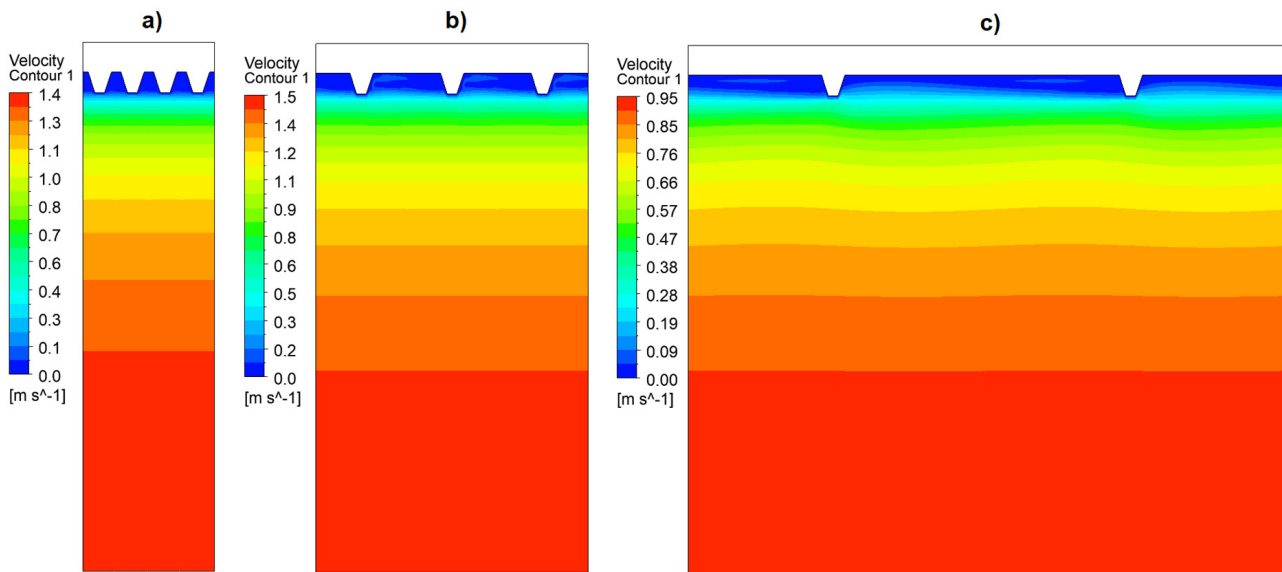


Figure 13. Velocity field for selected geometries at the same pressure gradient of 1000 [Pa/m]: (a) X2, (b) X5, and (c) X7.

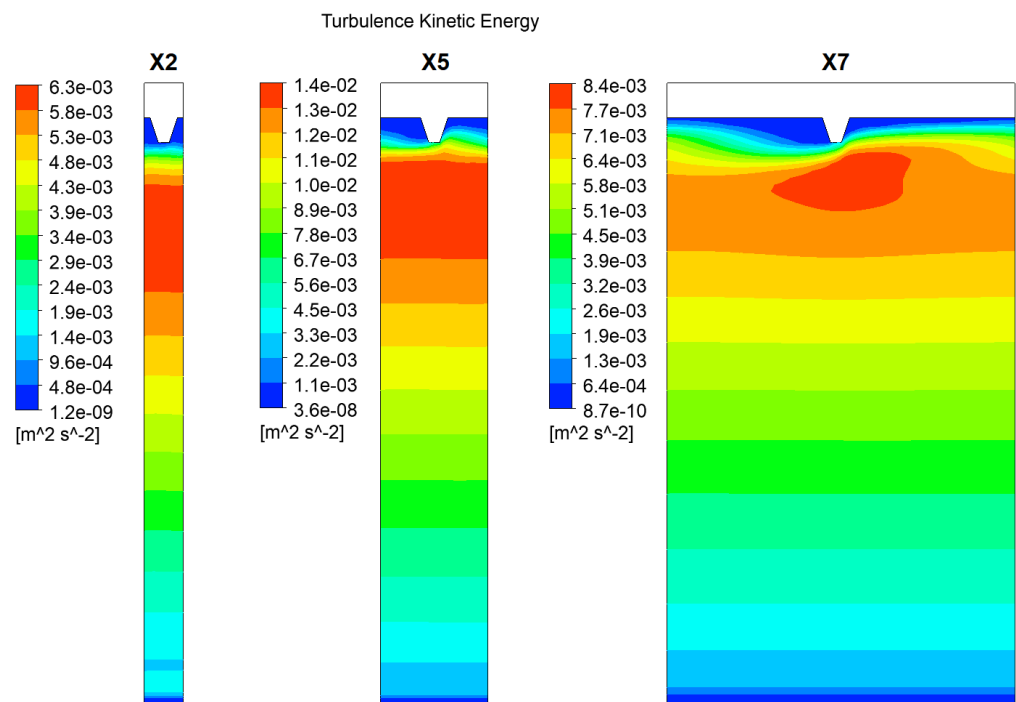


Figure 14. Turbulence Kinetic Energy (TKE) for selected geometries, X2, X5, and X7, at the same pressure gradient of 1000 [Pa/m].

Figure 15 shows the distribution of the Turbulence Eddy Dissipation (TED) parameter, which is a measure of the conversion of turbulence energy to internal thermal energy. Its largest values for each of the geometries studied are found in the area in close proximity to the top of the micro-fins. For the X5 and X7 geometries, i.e., for larger distances between the micro-fins, the highest TED values are observed in the small area just near the top of the micro-fins. On the other hand, for small inter-fin distances, like the X2 geometry, the highest energy dissipation also takes place near the top of the micro-fins but is extended over the entire length of the domain (yellow–green color). In general, TED is high in regions where the micro-fins interact with and disrupt the flow, also causing an increase in turbulence.

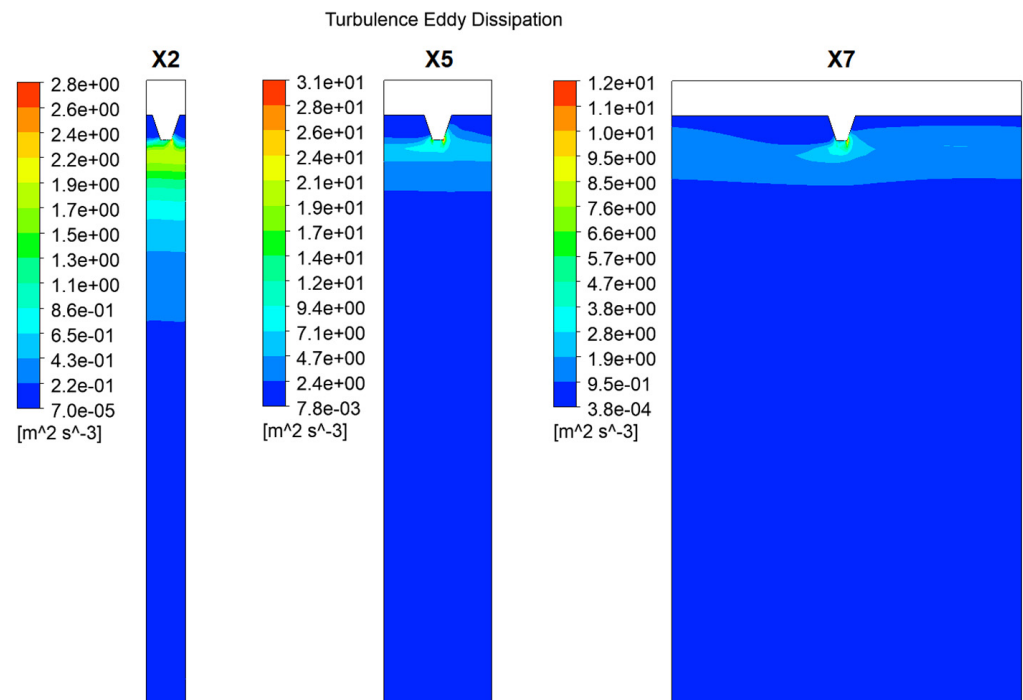


Figure 15. Turbulence Eddy Dissipation (TED) for selected geometries, X2, X5, and X7, at the same pressure gradient of 1000 [Pa/m].

It is known that the purpose of using micro-fins is to intensify the heat transfer between the fluid and the pipe wall, but this process is inherently associated with increased flow resistance, which is an unfavorable phenomenon because it increases the power requirement to pump the fluid. Therefore, criteria are used to evaluate such a channel in terms of the ratio of the benefit obtained from intensifying the heat transfer to the increasing flow resistance. One such parameter is the *PEC* (performance evaluation criteria) coefficient, which was calculated for the tested pipes from Equation (9). This parameter combines Nu and the friction factor obtained from the studies of channels with geometries other than a smooth pipe with Nu and the friction factor calculated for a smooth pipe at the same Reynolds number. The *PEC* coefficient is an indicator that indicates how much the heat transfer of the tested channel will increase compared to a smooth pipe with the same pumping power. *PEC* values above unity indicate a greater impact of heat transfer intensification than flow resistance, while values below unity indicate greater flow resistance in relation to the benefit obtained from the heat transfer intensification of the tested geometry.

Figure 16 shows the *PEC* coefficient for each geometry as a function of Re , while Figure 17 also shows the *PEC* coefficient but as a function of the longitudinal spacing of the micro-fins corresponding to the geometries X1, . . . X9.

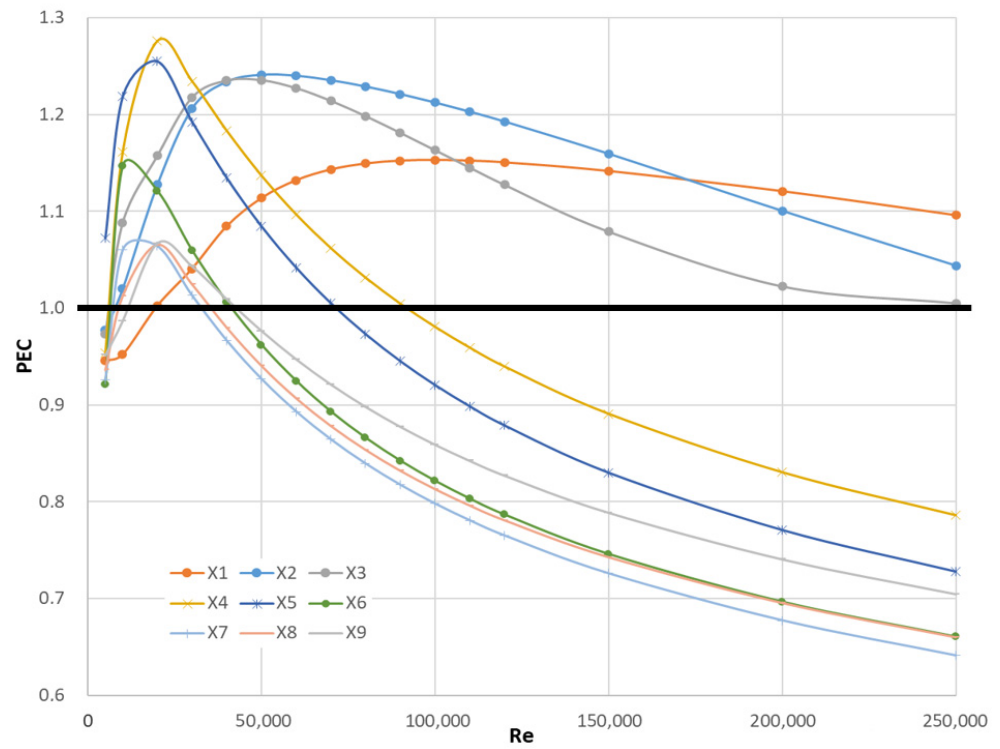


Figure 16. PEC coefficient for each tested geometry as a function of Re — $PEC(Re)$.

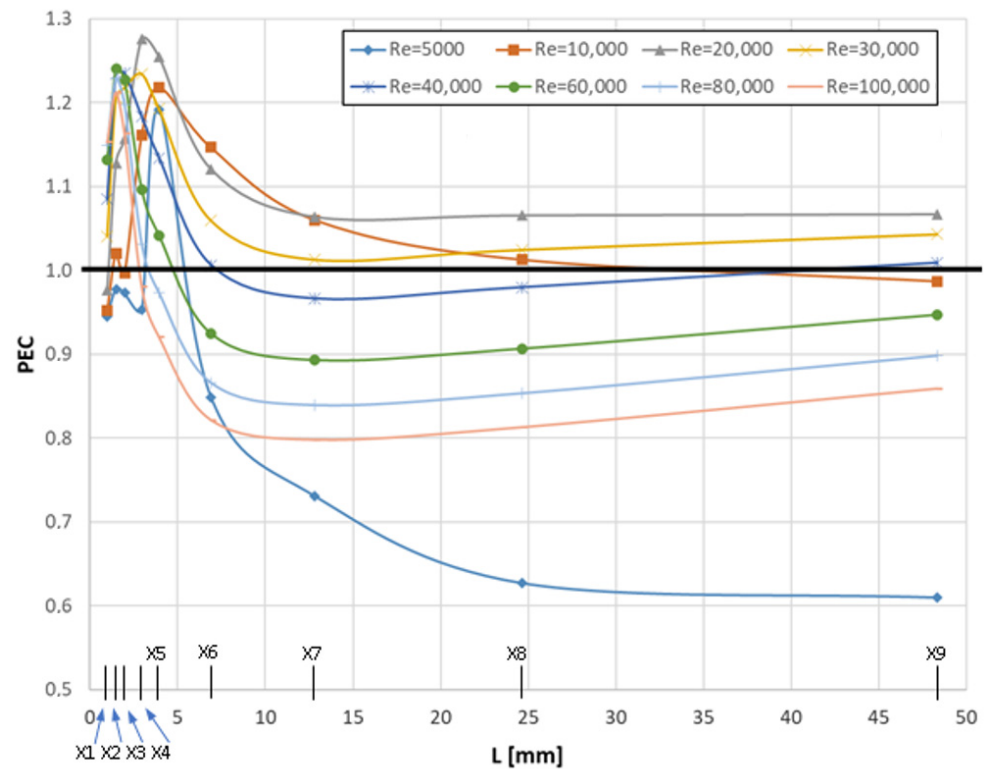


Figure 17. PEC coefficient for selected values of Re as a function of the longitudinal spacing of micro-fins— $PEC(L)$.

4. Discussion

The article presents the validation of the numerical model by comparing experimental data for a pipe with helical micro-fins with a height of $H = 0.25$ mm with data from the

numerical model. The maximum discrepancies between the experiment and the obtained numerical results are for a flow resistance of approximately 7% and for a Nusselt number of approximately 12%, as shown in Figure 2.

The friction factor obtained from the numerical tests for various longitudinal spacings of micro-fins was compared (Figure 9) with that of a smooth pipe, for which f_t was calculated according to the Blasius Formula (5). For each pipe with micro-fins, the obtained f_t values are higher than those for the smooth pipe, which indicates the physical correctness of the results. For $Re = 5000 \div 20,000$, the lowest friction factor values were recorded for the X3 geometry with a micro-fin spacing of $L = 0.555$ mm, and for Reynolds numbers above 25,000, they were recorded for the X1 geometry, i.e., for the pipe with the smallest micro-fin spacing. In turn, the highest f_t values in the entire Re number range were achieved by two geometries, X6 and X7, with micro-fin spacings of $L = 1934$ mm and $L = 3598$ mm, respectively. Generally, the friction factor of the studied geometries initially decreases with increasing Reynolds numbers, reaching a local minimum, and then increases. In Figure 9, this quite clear trend can be seen for all the studied geometries. Thus, it can be concluded that for each geometry, there is a certain range of Re in which f_t reaches its minimum and which is the most favorable in terms of flow resistance.

All the tested pipes had the same relative roughness of $\varepsilon = 0.02$, depending on the height of the micro-fins. Figure 9 shows a complete lack of agreement between the characteristics obtained from the numerical simulations and the curve calculated theoretically based on the well-known Formula (12) for the same relative roughness. Therefore, one of the key conclusions resulting from the numerical tests is the lack of correlation between the theoretically calculated friction factor (for irregular asperities) and the one obtained from studies (for the same roughness but with regular shapes). The same fact was noticed in research by Wang et al. [28].

Analyzing the heat transfer for the tested geometries, it can be observed that the highest values of Nu are noticed for the X5 geometry at $Re < 70,000$ and for X2 at $Re > 70,000$. The presented results show an irregular order in the position of the Nusselt number characteristics for different flow rates (Figure 11).

The analysis of the TKE and TED turbulence parameters, shown in Figures 14 and 15, can be an additional and complementary source of information about the flow and heat processes taking place in the pipe geometry under consideration, but there would have to be a clear correlation between them and flow resistance and heat transfer for them to be used in engineering applications.

As can be seen in Figure 16, for three geometries, X1, X2, and X3, in almost the entire range of Re , the PEC coefficient is greater than unity, apart from for very small Re . For the remaining geometries, there is a very clear maximum in the range of $Re = 10,000\text{--}30,000$, reaching the highest value of $PEC = 1.28$ for X4, and then rapidly decreasing to values below 1 for larger Re values. Figure 17 shows the dependence of the PEC coefficient as a function of the longitudinal spacing of the micro-fins, L (markers of the geometry names to which this spacing corresponds are also plotted on the horizontal axis), for selected Re values. Here, in turn, it can be seen that for the geometries X1 to X5, i.e., with the smallest micro-fin spacings and for Re up to 100,000, the PEC values are greater than unity.

5. Conclusions

Based on the numerical research presented in this article, the most important conclusions of this work can be presented:

- A numerical model was built and verified with experimental data.
- Mathematical correlations reflecting the nature of changes in the friction factor and Nusselt number as a function of the Reynolds number were determined for the studied longitudinal distances of the micro-fins.
- Using the PEC (performance evaluation criteria) method for assessing the thermal efficiency of the flow channels, the highest values were observed for micro-fins with a spacing of $L = 0.831$ mm and $L = 1.107$ mm, i.e., for the X4 and X5 geometries.

- A lack of compliance between the theoretical formulas for the friction factor for rough pipes (Moody's diagram) and the obtained numerical results for the same relative roughness but with a regular shape was observed.
- The use of this type of micro-fin is most justified in terms of the heat transfer efficiency for the X4 and X5 geometries in the Reynolds number range of $Re = 20,000\text{--}30,000$, as well as for the X2 and X3 pipes in the range of $Re = 30,000\text{--}120,000$.

Funding: This research received no external funding.

Data Availability Statement: Data are contained within the article.

Conflicts of Interest: The author reports no conflicts of interest.

Nomenclature

A_{wall}	outside surface of wall [m ²];
D	diameter [mm];
ft	friction factor [-];
ft_s	friction factor for smooth tube [-];
$\text{grad}p$	pressure gradient [Pa/m]
h	heat transfer coefficient [W/m ² K];
e	height of micro-fin [mm];
k	thermal conductivity [W/mK];
L	distance between micro-fins [m];
Nu	Nusselt number [-];
Nu_s	Nusselt number for smooth tube [-];
PEC	performance evaluation criteria [-];
Δp	pressure drop [Pa];
Pr	Prandtl number [-];
q	wall heat flux [W/m ²]
Re	Reynolds number [-];
T_w	wall pipe temperature [K];
T_b	bulk temperature [K];
u_{av}	average velocity [m/s];
V_{FD}	volume of fluid domain [m ³]
ε	relative roughness [-]

References

1. Jasiński, P.B. Numerical study of the thermo-hydraulic characteristics in a circular tube with ball turbulators. Part 1: PIV experiments and a pressure drop. *Int. J. Heat Mass Transf.* **2014**, *74*, 48–59. [[CrossRef](#)]
2. Jasiński, P.B. Numerical study of the thermo-hydraulic characteristics in a circular tube with ball turbulators. Part 2: Heat transfer. *Int. J. Heat Mass Transf.* **2014**, *74*, 473–483. [[CrossRef](#)]
3. Jasiński, P.B. Numerical study of thermo-hydraulic characteristics in a circular tube with ball turbulators. Part 3: Thermal performance analysis. *Int. J. Heat Mass Transf.* **2017**, *107*, 1138–1147. [[CrossRef](#)]
4. Wijayanta, A.T.; Pranowo; Mirmanto; Kristiawan, B.; Aziz, M. Internal flow in an enhanced tube having square-cut twisted tape insert. *Energies* **2019**, *12*, 306. [[CrossRef](#)]
5. Triwijayanta, A.; Aziz, M.; Kariya, K.; Miyara, A. Article numerical study of heat transfer enhancement of internal flow using double-sided delta-winglet tape insert. *Energies* **2018**, *11*, 3170. [[CrossRef](#)]
6. Kristiawan, B.; Wijayanta, A.T.; Enoki, K.; Miyazaki, T.; Aziz, M. Heat transfer enhancement of TiO₂/water nanofluids flowing inside a square minichannel with a microfin structure: A numerical investigation. *Energies* **2019**, *12*, 3041. [[CrossRef](#)]
7. Asirvatham, L.G.; Vishal, N.; Gangatharan, S.K.; Lal, D.M. Experimental study on forced convective heat transfer with low volume fraction of CuO/Water nanofluid. *Energies* **2009**, *2*, 97–119. [[CrossRef](#)]
8. Patil, M.S.; Seo, J.H.; Kang, S.J.; Lee, M.Y. Review on synthesis, thermo-physical property, and heat transfer mechanism of nanofluids. *Energies* **2016**, *9*, 840. [[CrossRef](#)]
9. Study, A.E.; Shajahan, M.I.; Michael, J.J.; Arulprakasajothi, M.; Suresh, S. Effect of Conical Strip Inserts and ZrO₂/DI-Water Nanofluid on Heat Transfer Augmentation: An Experimental Study. *Energies* **2020**, *13*, 4554.
10. Virgilio, M.; Mayo, I.; Dedeyne, J.; Van Geem, K.M.; Marin, G.B.; Arts, T. Effects of 2-D and 3-D helical inserts on the turbulent flow in pipes. *Exp. Therm. Fluid Sci.* **2020**, *110*, 109923. [[CrossRef](#)]

11. Ji, W.T.; Zhang, D.C.; He, Y.L.; Tao, W.Q. Prediction of fully developed turbulent heat transfer of internal helically ribbed tubes—An extension of Gnielinski equation. *Int. J. Heat Mass Transf.* **2012**, *55*, 1375–1384. [[CrossRef](#)]
12. Córcoles, J.I.; Moya-Rico, J.D.; Molina, A.E.; Almendros-Ibáñez, J.A. Numerical and experimental study of the heat transfer process in a double pipe heat exchanger with inner corrugated tubes. *Int. J. Therm. Sci.* **2020**, *158*, 106526. [[CrossRef](#)]
13. Al-Obaidi, A.R.; Alhamid, J. Investigation of flow pattern, thermohydraulic performance and heat transfer improvement in 3D corrugated circular pipe under varying structure configuration parameters with development different correlations. *Int. Commun. Heat Mass Transf.* **2021**, *126*, 105394. [[CrossRef](#)]
14. Al-Obaidi, A.R.; Alhamid, J. Investigation of the effect of various corrugated pipe configurations on thermo-hydraulic flow and enhancement of heat transfer performance with the development of different correlations. *Int. J. Therm. Sci.* **2022**, *176*, 107528. [[CrossRef](#)]
15. Dastmalchi, M.; Sheikhzadeh, G.A.; Arefmanesh, A. Optimization of micro-finned tubes in double pipe heat exchangers using particle swarm algorithm. *Appl. Therm. Eng.* **2017**, *119*, 1–9. [[CrossRef](#)]
16. Dastmalchi, M.; Arefmanesh, A.; Sheikhzadeh, G.A. Numerical investigation of heat transfer and pressure drop of heat transfer oil in smooth and micro-finned tubes. *Int. J. Therm. Sci.* **2017**, *121*, 294–304. [[CrossRef](#)]
17. Jasiński, P. Numerical optimization of flow-heat ducts with helical micro-fins, using entropy generation minimization (EGM) method. In Proceedings of the 9th IASME/WSEAS International Conference on Fluid Mechanics & Aerodynamics (FMA' 11), Florence, Italy, 23–25 August 2011; pp. 47–54.
18. Li, X.; Meng, J.; Li, Z. Roughness enhanced mechanism for turbulent convective heat transfer. *Int. J. Heat Mass Transf.* **2011**, *54*, 1775–1781. [[CrossRef](#)]
19. Brognaux, L.J.; Webb, R.L.; Chamra, L.M.; Chung, B.Y. Single-phase heat transfer in micro-fin tubes. *Int. J. Heat Mass Transf.* **1997**, *40*, 4345–4357. [[CrossRef](#)]
20. Zawadzki, A.; Plocek, M.; Kapusta, T.; Kasieczka, W. Heat transfer and friction factor characteristics of single-phase flow through a circular, internally micro-finned, horizontal tube fitted with twisted tape inserts—Experimental investigations. In Proceedings of the XL Refrigeration Days, Poznań, Poland, 15–17 October 2008; pp. 115–124. (In Polish)
21. Liao, W.; Lian, S. Effect of compound corrugation on heat transfer performance of corrugated tube. *Int. J. Therm. Sci.* **2023**, *185*, 108036. [[CrossRef](#)]
22. Manual ANSYS-CFX. Available online: <http://www.ansys.com> (accessed on 1 March 2018).
23. Di Piazza, I.; Ciofalo, M. Numerical prediction of turbulent flow and heat transfer in helically coiled pipes. *Int. J. Therm. Sci.* **2010**, *49*, 653–663. [[CrossRef](#)]
24. Eiamsa-ard, S.; Wongcharee, K.; Sripattanapipat, S. 3-D Numerical simulation of swirling flow and convective heat transfer in a circular tube induced by means of loose-fit twisted tapes. *Int. Commun. Heat Mass Transf.* **2009**, *36*, 947–955. [[CrossRef](#)]
25. Celik, I.B.; Ghia, U.; Roache, P.J.; Freitas, C.J.; Coleman, H.; Raad, P.E. Procedure for estimation and reporting of uncertainty due to discretization in CFD applications. *J. Fluids Eng. Trans. ASME* **2008**, *130*, 78001–78004.
26. Moody, L.F. Friction Factors for Pipe Flow. *Trans. Am. Soc. Mech. Eng.* **1944**, *66*, 671–681. [[CrossRef](#)]
27. Swamee, P.K.; Jain, A.K. Explicit equations for pipe-flow problems. *J. Hydraul. Div.* **1976**, *102*, 657–664. [[CrossRef](#)]
28. Wang, C.C.; Chiou, C.B.; Lu, D.C. Single-phase heat transfer and flow friction correlations for microfin tubes. *Int. J. Heat Fluid Flow* **1996**, *17*, 500–506. [[CrossRef](#)]

Disclaimer/Publisher's Note: The statements, opinions and data contained in all publications are solely those of the individual author(s) and contributor(s) and not of MDPI and/or the editor(s). MDPI and/or the editor(s) disclaim responsibility for any injury to people or property resulting from any ideas, methods, instructions or products referred to in the content.